Graphene Heterostructure Integrated Optical Fiber Bragg Grating for Light Motion Tracking and Ultrabroadband Photodetection from 400 nm to 10.768 μm

Article *in* Advanced Functional Materials · March 2019

DOI: 10.1002/adfm.201807274

CITATIONS
3

READS
195

14 authors, including:

Dr. Shivananju B N
Monash University (Australia)
48 PUBLICATIONS **508** CITATIONS
SEE PROFILE

Wenzhi Yu
Soochow University (PRC)
28 PUBLICATIONS **388** CITATIONS
SEE PROFILE

Haoran Mu
Monash University (Australia)
24 PUBLICATIONS **838** CITATIONS
SEE PROFILE

Sun Tian
Soochow University (PRC)
11 PUBLICATIONS **158** CITATIONS
SEE PROFILE

ADVANCED FUNCTIONAL MATERIALS
www.afm-journal.de

Graphene Heterostructure Integrated Optical Fiber Bragg Grating for Light Motion Tracking and Ultrabroadband Photodetection from 400 nm to 10.768 µm

Bannur Nanjunda Shivananju, Xiaozhi Bao, Wenzhi Yu, Jian Yuan, Haoran Mu, Tian Sun, Tianyu Xue, Yupeng Zhang, Zhongzhu Liang, Ruifeng Kan, Han Zhang, Bo Lin, Shaojuan Li,* and Qiaoliang Bao**

Integrated photonics and optoelectronics devices based on graphene and related 2D materials are at the core of the future industrial revolution, facilitating compact and flexible nanophotonic devices. Tracking and detecting the motion of broadband light in millimeter to nanometer scale is an unfold science which has not been fully explored. In this work, tracking and detecting the motion of light (millimeter precision) is first demonstrated by integrating graphene with an optical fiber Bragg grating device (graphene-FBG). When the incident light moves toward and away from the graphene-FBG device, the Bragg wavelength red-shifts and blue-shifts, indicating its light motion tracking ability. Such light tracking capability can be further extended to an ultrabroad wavelength range as all-optical photodetectors show the robust response from 400 nm to 10.768 µm with a linear optical response. Interestingly, it is found that graphene-Bi_2Te_3 heterostructure on FBG shows 87% higher photoresponse than graphene-FBG at both visible and telecom wavelengths, due to stronger phonon-electron coupling and photo-thermal conversion in the heterostructure. The device also shows superior stability even after 100 d. This work may open up amazing integrated nanophotonics applications such as astrophysics, optical communication, optical computing, optical logic gating, spectroscopy, and laser biology.

1. Introduction

The ability to detect the motion of light from millimeter to nanometer (mm to nm) scale is an unfold science which may lead to novel photonics devices such as wavelength tuner, filters, modulators, and material characterization based on the light motion. Various techniques have been demonstrated to detect the motion of sun light from centimeter to meter (cm to m) scale using mechanical and electrical methods for energy harvesting.[1] The mechanical approach was developed for detect the motion of sunlight by using polymer, semiconductor, and ceramic which undergo strain under light illumination similar to the sunflower.[2] Recently, Gariepy et al. developed a camera based on silicon avalanche diodes array which is capable of observing light-in-flight.[3] However, it will take about an hour to take enough shots to make a final video representing the motion of light.[3] Besides, silicon is restricted to specific wavelength

Dr. B. N. Shivananju, X. Bao, Dr. T. Xue, Dr. Y. Zhang, Prof. H. Zhang, Prof. Q. Bao
College of Electronic Science and Technology and College of Optoelectronics Engineering
Collaborative Innovation Centre for Optoelectronic Science and Technology and Key Laboratory of Optoelectronic Devices and Systems of Ministry of Education and Guangdong Province
Shenzhen University
Shenzhen 518000, P. R. China
E-mail: qlbao@szu.edu.cn

Dr. B. N. Shivananju, W. Yu, H. Mu, Dr. Y. Zhang, Prof. Q. Bao
Department of Materials Science and Engineering
ARC Centre of Excellence in Future Low-Energy Electronics Technologies (FLEET)
Monash University
Clayton, Victoria 3800, Australia
E-mail: qiaoliang.bao@monash.edu

The ORCID identification number(s) for the author(s) of this article can be found under https://doi.org/10.1002/adfm.201807274.

Dr. B. N. Shivananju, Dr. J. Yuan, T. Sun, Dr. S. Li, Prof. Q. Bao
Institute of Functional Nano and Soft Materials (FUNSOM)
Jiangsu Key Laboratory for Carbon-Based Functional Materials and Devices
Soochow University
Suzhou 215123, P. R. China
E-mail: sjli@suda.edu.cn

Dr. Z. Liang, Prof. R. Kan
State Key Laboratory of Applied Optics
Changchun Institute of Optics
Fine Mechanics and Physics
Chinese Academy of Sciences
Changchun, Jilin 130033, China

Prof. B. Lin
China Academy of Electronics and Information Technology
Beijing 100041, China
E-mail: bolin_academic@163.com, linbo5@cetc.com.cn

DOI: 10.1002/adfm.201807274

and limited to narrowband photodetection. These light tracking systems have been hampered detecting the motion of broadband light from millimeter to nanometer (mm to nm) scale in real time and cannot be used to tune the optical wavelength in nanophotonics devices. It is nontrivial to seek for new solutions which can integrate emerging materials with new optical devices to deliver superior light tracking capabilities.

Recently, 2D materials such as graphene, topological insulators, transition metal dichalcogenides, and black phosphorous have revealed their incredible improvements in the field of optoelectronics and photonics applications[4–9] such as ultrafast lasers,[10,11] broadband photodetectors,[12–14] high-performance light-emitting diodes (LEDs),[15] ultrafast optical modulators,[16,17] broadband polarizers,[18] and high quantum efficiency plasmonic devices.[19,20] Due to their good flexibility, 2D materials could also be easily integrated with optical fibers to realize all-optical operation,[17,21] which offers attractive advantages in structural miniaturization, resistance to electromagnetic interference, highly multiplexing ability, noncontact, long-term stability, and remote use. The recent progress on the ultrafast all-optical modulators[16,17,21] and the ultrasensitive optical biochemical sensors[22] implies intriguing potential for highly sensitive photosignal sensing and light modulation based on 2D materials integrated optical fiber.

In this work, we demonstrated the tracking of light motion based on 2D materials integrated optical fiber Bragg grating (FBG) device. Broadband wavelength response of graphene due to its zero bandgap nature and nanoscaled Bragg gratings in optical fiber afford the capability to detect the ultrabroadband light from 400 nm to 10.768 μm with linear photoresponse (far better than electrical devices). We further demonstrated that graphene-Bi_2Te_3 heterostructure integrated FBG device shows enhanced light detection with the ultrahigh photoresponse than that of graphene integrated FBG device.

2. Results and Discussions

2.1. Tracking the Motion of Light

The experimental setup for light motion tracking and detecting is schematically shown in **Figure 1**a. The fabrication process of the chemical vapor deposition (CVD) grown graphene[23,24] on to the FBG device is explained in detail in Figure S1 in the Supporting Information. An optical image at the bottom right in Figure 1a shows single-mode optical FBG wrapped by single-layer graphene. To confirm the high quality of the monolayer graphene, Raman spectroscopy was performed and the result is shown in Figure S2 in the Supporting Information. Broadband light from the supercontinuum laser source is pumped into the graphene-FBG device, and the reflected light by the Bragg gratings at a wavelength of ≈1546 nm is collected through a circulator and analyzed by using an optical spectrum analyzer (OSA). When the broadband light is guided into the FBG, one part of the light is reflected back with a particular wavelength which is called Bragg wavelength (λ_B) and the other part transmits through the core of the FBG.[25–28] The Bragg wavelength (λ_B) is correlated with the grating period in between the grating pitches inside the FBG and can be written as following[25,26]

$$\Delta \lambda_B = 2 n_{eff} \Lambda \tag{1}$$

where λ_B is the function of the effective refractive index (n_{eff}) and the period of the grating pitch (Λ)[25,26] inscribed in the optical fiber core.

Figure 1b,c illustrates the schematics of Bragg wavelength shift ($\Delta\lambda_B = \lambda_{B,illumination} - \lambda_{B,dark}$) of the device under light illumination. When incident light is illuminated on graphene, photoinduced carriers (electron–hole pairs) are generated due to strong light-matter interaction in graphene film. We can also expect to see the relaxation of photocarriers in graphene because there is no channel for the photoinduced carriers to be extracted out in our FBG system. Specifically, strong phonon–electron coupling in graphene would convert into Joule heating (here we refer it as photothermal (ΔT) effect) due to the zero bandgap in graphene.[12,29,30]

The photothermal heat deposited in the optical fiber cladding quickly conducts through the ultrathin silica to the fiber core, with its coefficient of thermal conductance K_{clad} = 1.4 W m^{-1} K^{-1} and thus modulate the Bragg gratings parameters (n_{eff} and Λ). The Bragg wavelength shift $\Delta\lambda_B$ in an FBG device induced by thermal effect (a temperature change ΔT) can be derived by Equation (2)[31,32]

$$\Delta \lambda_B = 2\left(\Lambda \frac{\partial n}{\partial T} + n \frac{\partial \Lambda}{\partial T}\right)\Delta T \tag{2}$$

where $n\frac{\partial \Lambda}{\partial T}$ denotes the variation in the grating pitch and $\Lambda\frac{\partial n}{\partial T}$ represents the variation in the effective refractive index due to a light induced temperature change ΔT. Thereby, Bragg wavelength shift $\Delta\lambda_B$ at a light induced temperature variation ΔT can be formulated by below equation[30,31]

$$\Delta \lambda_B = \lambda_B (\alpha + \zeta) \Delta T \tag{3}$$

where ζ is the thermo-optic coefficient (8.6×10^{-6}) and α is the thermal expansion coefficient (0.55×10^{-6}). We need to point out that the Bragg wavelength shift $\Delta\lambda_B$ due to thermo-optic effect (ζ) is 15.6 times higher than thermal expansion effect (α).[31,32] Based on the above theoretical equations, we can conclude that the Bragg wavelength shift $\Delta\lambda_B$ in graphene-FBG device is mainly due to photoinduced thermo-optic effect (change in Δn_{eff})[31,32] and this provides a novel means for photodetection with ultrahigh sensitivity and ultrabroadband spectral response.

Next we turn our attention on the change of the Bragg wavelength shift $\Delta\lambda_B$ as the incident light moves across the graphene-FBG device. The corresponding experimental setup is shown in Figure 1d. Collimated green laser (532 nm) with the power of 1.6 mW and beam waist of 3 mm is used as light source which moves across the graphene-FBG device with the help of displacement stage. As the collimated laser spot moves across the graphene-FBG, we can also observe linear motion of the diffracted light from the graphene-FBG device in the scale. This motion of the light in millimeter (mm) precision can be instantly monitored by graphene-FBG device. The pictorial representation of the graphene-FBG device used to track the motion of light with the displacement of several millimeters (mm)

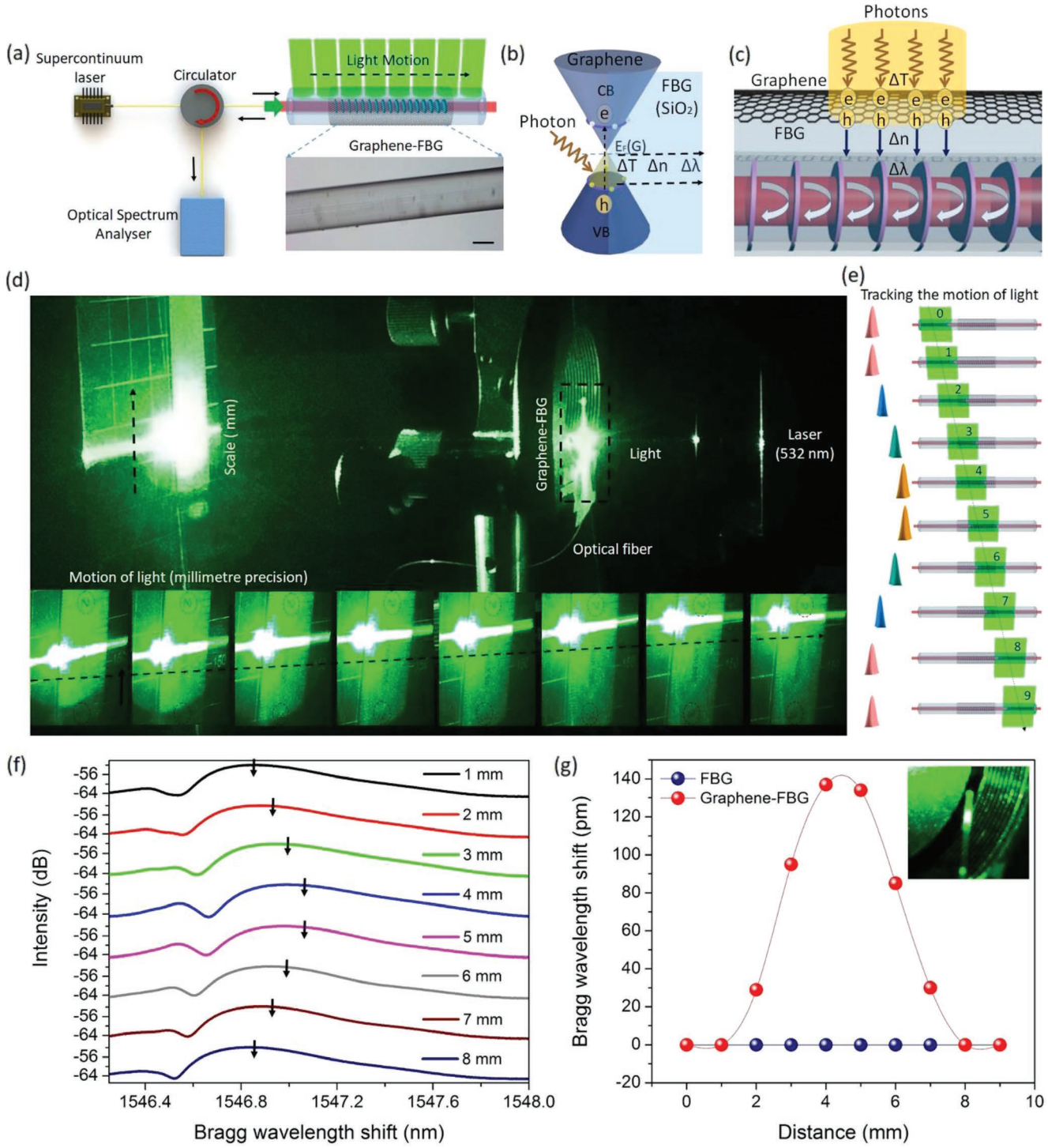

Figure 1. Tracking the motion of light based on graphene-FBG device. a) Schematic diagram of experimental setup for light motion tracking and detecting. An optical image at the bottom right shows graphene-FBG device. Scale bar, 50 µm. b) The band energy diagram of the graphene-FBG device and the photoexcited hot carrier transport process under illumination. c) The photoinduced electrons and holes generation in graphene and resulting in shift in the Bragg wavelength of FBG. d) Optical images showing the experiment setup for detecting the motion of light in millimeter (mm) precision. Collimated green laser with a wavelength of 532 nm is used as light source which moves across the graphene-FBG device. Inset: As the collimated laser spot moves across the graphene-FBG, we can also observe linear motion of diffracted green light in the scale. e) Schematic diagram of the shift in the Bragg wavelength of graphene-FBG when the light moves across Bragg gratings. f) The shift in the Bragg wavelength increases and decreases when the light moves toward and away from the graphene-FBG device. g) The shift in the Bragg wavelength with respect to distance (mm) when the light moves across the graphene-FBG device and compared with bare FBG. Inset: Optical image showing the motion of light on graphene-FBG device.

across the Bragg gratings is shown in Figure 1e. When external photons are incident on the graphene-FBG device, we are able to observe the Bragg wavelength shift $\Delta\lambda_B$. Figure 1f exhibits the change in the Bragg wavelength when the incident light moves across the graphene-FBG device for a distance of 8 mm. We are able to observe the Bragg wavelength redshifts and blueshifts when the light moves toward and away from the graphene-FBG device with respect to distance (mm) as shown in Figure 1g (red color). The inset of Figure 1g shows an optical image of the motion of light on graphene-FBG device. When the incident light contacts with the bare optical fiber portion that is without graphene-FBG (see the points 0 and 9 marked in Figure 1e), there was no spectral shift in the Bragg wavelength (till distance 1 mm, see Figure 1e). But whenever the light motion comes in contact with both the graphene and the Bragg gratings portion (at distance 2 mm), there shows a corresponding slight Bragg wavelength shift $\Delta\lambda_B$ due to the light induced thermo-optic effect (photothermal-optic effect). As the laser spot moves over a larger portion across the graphene-FBG, we can observe linear increase in shift in the Bragg wavelength (distance 2–4 mm). The Bragg wavelength shift $\Delta\lambda_B$ starts decreasing linearly when the laser beam starts moving away from the graphene-FBG (distance 5–7 mm) and then comes back to initial Bragg wavelength (distance 8 mm) when the laser beam is no more interacting with the graphene-FBG device. In comparison, we repeated this experiment with bare FBG without graphene coated, and we were not able to observe any obvious spectral shift in the Bragg wavelength when the green laser spot (532 nm, 1.6 mW) moves across the Bragg gratings (blue dots in Figure 1g). This experimental result proves that both graphene and the Bragg gratings plays a key role for tracking the motion of light and it can be extended for tracking and detecting the broadband light (visible to far-infrared). The ability to detect the motion of light in millimeter (mm) scale may lead to novel photonics devices such as wavelength tuner, filters, and modulators based on the light motion.

2.2. Ultrabroadband Photoresponse of Graphene-FBG Device

Figure 2 shows the ultrabroadband (400 nm to 10.768 μm) photodetection of the graphene-FBG device at room temperature. Figure 2a displays the schematic diagram of the ultrabroadband wavelength photoresponse of graphene-FBG device. When incident light of different wavelengths are illuminated on the graphene-FBG surface, electron–hole pairs are generated and the strong phonon–electron coupling in graphene results in photothermal effect, resulting in refractive index change (Δn_{eff}) in FBG device which leads to the Bragg wavelength shift $\Delta\lambda_B$, as discussed above. Figure 2b shows the experimental results of ultrabroadband wavelength response of graphene-FBG photodetector which covers visible (400, 532, and 635 nm), near-infrared (980 and 1550 nm), mid-infrared (4.67 μm), and far-infrared (7.26 and 10.768 μm) wavelengths. The optical images of the experimental setup used to carry out the ultrabroadband photodetection measurements are shown in Figure S3 in the Supporting Information. We could clearly observe more than 100 pm shift in the Bragg wavelength for all incident light from 400 nm to 10.768 μm (Figure 2b). Notably, the shift in the Bragg wavelength at 400 nm is slightly higher than other wavelengths. Similarly in the UV–vis–IR spectrum (Figure S4, Supporting Information), we could observe slight increase in the absorption of graphene for wavelength less than 500 nm, due to hydrocarbon contamination.[6] Based on our knowledge, our results show the widest range of wavelengths (400 nm to 10.768 μm) response compared to all the photodetectors reported till now based on graphene and related 2D materials.[12,13,33,34]

Figure 2c,d shows the power dependence (10^{-6}–10^{-3} W) of linear Bragg wavelength shift $\Delta\lambda_B$ measured at graphene-FBG device for ultrabroadband wavelengths (400 nm to 10.768 μm). The Bragg wavelength shift increases with promoting the incident light power, which can be attributed to the increased number of photoinduced carriers, and thus enhanced phonon–electron coupling (photothermal) effect at higher illumination power. The observed Bragg wavelength shift depends linearly on the illumination power. Notably, the graphene-FBG device shows linear photoresponse better than that of graphene integrated electrical photodetectors.[12,33] The reliable output Bragg wavelength shift and incident optical power over ultrabroadband spectral range (400 nm to 10.768 μm) makes graphene-FBG based photodetectors ideally suitable to astrophysics, radiometry, bolometer, optical communication, spectroscopy, laser biology, and sensing applications. The maximum photosensitivity of graphene-FBG device was found to be 95 pm mW^{-1} with the limit of detection (LoD) of 210 μW (LoD = resolution of the OSA (20 pm)/sensitivity (95 pm mW^{-1})). The LoD can be further reduced to nW by using high resolution interrogator system, using micro or etched FBG devices[35,36] and by increasing the absorption of graphene by constructing heterostructures with other 2D materials.

2.3. Graphene-Bi_2Te_3-FBG Heterostructure Broadband Photodetector

The combination of graphene with small bandgap 2D semiconducting materials seems to be more favorable approach for broadband light detection with increased photoresponse.[37] In this section, we also demonstrated ultrasensitive photoresponse based on graphene-Bi_2Te_3-FBG heterostructure from visible (400 nm) to telecom (1550 nm) wavelengths at room temperature. Layered Bi_2Te_3 rhombohedral crystals are small bandgap (≈0.15 eV) 2D material from topological insulator family.[37] The experimental setup of graphene-Bi_2Te_3-FBG heterostructure device is similar with the graphene-FBG device, as is shown in **Figure 3**a. The scanning electron microscopic (SEM) image at the bottom right in Figure 3a shows Bi_2Te_3 nanocrystals grown on the monolayer graphene substrate by CVD method and then transferred onto the optical FBG cladding surface. Here we use the graphene-Bi_2Te_3 heterostructure with a thickness of ≈30 nm. The Figure S5 in the Supporting Information displays the Raman spectroscopy of the graphene-Bi_2Te_3 heterostructure which endorses the presence of Bi_2Te_3 crystal on top of graphene monolayer. Figure 3b shows the schematic diagram of energy diagram proposed to illustrate the optical excitation and relaxation process of photocarriers in graphene-Bi_2Te_3-FBG heterostructure. Graphene is zero bandgap semimetal material,

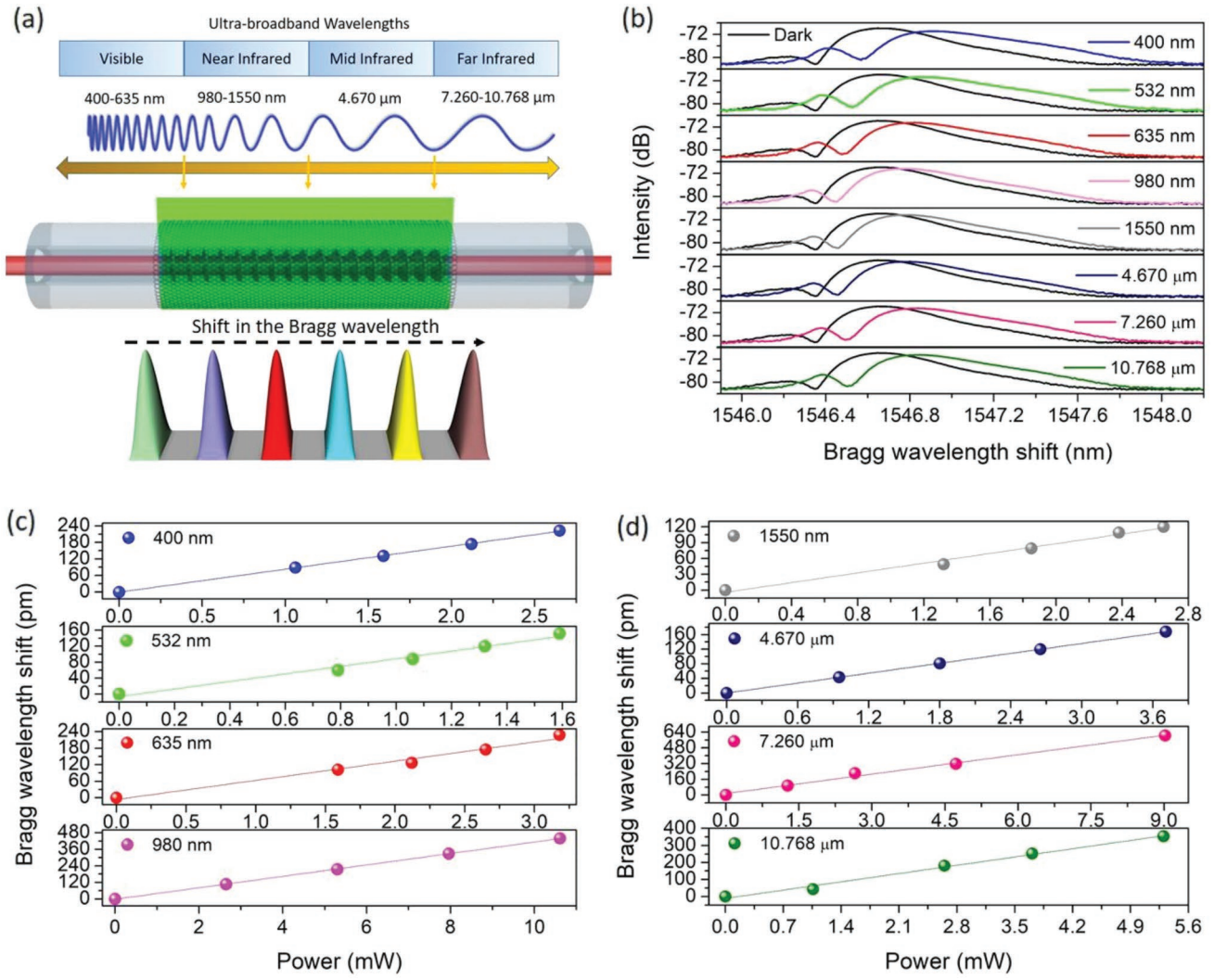

Figure 2. Ultrabroadband wavelength photoresponse of graphene-FBG device. a) Schematic diagram of the ultrabroadband photon illumination on graphene-FBG device and the shift in the Bragg wavelength. b) The redshift in the Bragg wavelength when the photon of different wavelengths (400 nm to 10.768 μm) illuminated on graphene-FBG device. c) The linear increase in shift in the Bragg wavelength of graphene-FBG as a function of the increase in the incident power of visible (400, 532, and 635 nm), and near infrared (980 nm) wavelengths. d) Telecom (1550 nm), mid-infrared (4.670 μm), and far-infrared (7.260 and 10.768 μm) wavelengths.

whereas Bi_2Te_3 has a very small bandgap (≈0.15 eV), which renders the hybrid system the strong broadband light absorption capability from visible to infrared wavelengths. When the light is illuminated on the graphene-Bi_2Te_3 heterostructure, the photon induced electrons–holes pairs are generated in both Bi_2Te_3 and graphene 2D materials, and electrons in Bi_2Te_3 transfer toward graphene and then after get relaxed in graphene, at the same time the photon induced holes in graphene will be transferred into Bi_2Te_3, preventing the direct recombination of electron–hole pairs.[38] As a result, the number of photon induced carriers in graphene-Bi_2Te_3 heterostructure are much higher than in pure graphene which leads to strong phonon–electron coupling in graphene-Bi_2Te_3 heterostructure would convert into photothermal effect and lead to higher Bragg wavelength shift.

Based on the above observation, we believe that Bi_2Te_3 play an import role for the increased shift in the Bragg wavelength. To verify this, Raman mapping measurements were performed on graphene-Bi_2Te_3 heterostructure. Figure 3c,d shows the optical image and the corresponding Raman mapping result of graphene-Bi_2Te_3 heterostructure. The Raman mapping is performed by focusing a visible laser (514 nm) light and scanned over the graphene-Bi_2Te_3 heterostructure. The Raman wavelength used during mapping locates at the characteristic G peak of graphene (Figure S5, Supporting Information). The graphene-Bi_2Te_3 heterostructure regions (indicated by blue color) and monolayer graphene (indicated by red or yellow color) can be clearly seen from the Raman mapping result, in accordance with the optical image. Figure 3e displays the broadband wavelength (350–1600 nm) absorption of pure graphene and graphene-Bi_2Te_3 heterostructure, which clearly shows that the graphene-Bi_2Te_3 heterostructure has enhanced light absorption (30%) than monolayer graphene (2.3%) due to the

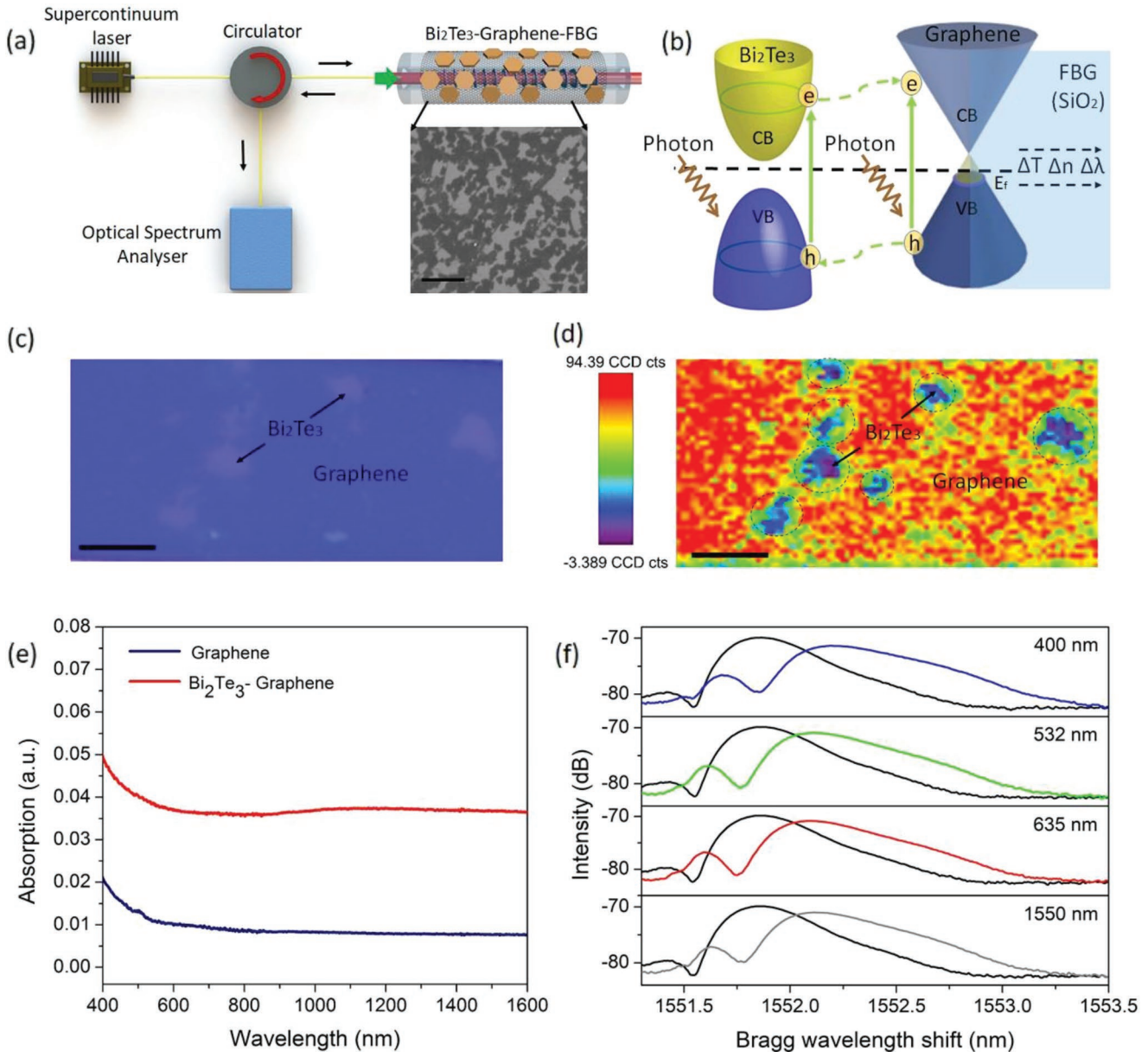

Figure 3. Graphene-Bi_2Te_3-FBG heterostructure device for broadband wavelength detection. a) Schematic diagram of experimental setup of graphene-Bi_2Te_3-FBG heterostructure photodetector. The inset is the scanning electron microscopic (SEM) image of Bi_2Te_3 nanoplatelets grown on graphene. Scale bar, 1 µm. b) The energy band diagram of graphene-Bi_2Te_3-FBG heterostructure device and the photoexcited hot carrier transport process under illumination; the dotted line represents the Fermi levels (E_F). c) Optical image of the graphene-Bi_2Te_3 heterostructure device. Scale bar, 8 µm. d) Scanning Raman mapping result of the graphene-Bi_2Te_3 heterostructure. Scale bar, 8 µm. e) The broadband absorption spectrum of graphene-Bi_2Te_3 heterostructure in comparison with monolayer graphene. f) The redshift in the Bragg wavelength when the photon of different wavelengths (400 to 1550 nm) illuminated on graphene-Bi_2Te_3-FBG heterostructure device.

strong light absorption of Bi_2Te_3. Therefore, graphene-Bi_2Te_3-FBG heterostructure has much larger Bragg wavelength shift than graphene-FBG at both visible and infrared wavelengths. Figure 3f shows the Bragg wavelength shift when incident light of different wavelengths (400, 532, 635, and 1550 nm) are illuminated on graphene-Bi_2Te_3-FBG heterostructure. This shows the potential of graphene-Bi_2Te_3-FBG heterostructure for broadband light detection including at the telecom wavelength (1550 nm).

2.4. Power-Dependent Photoresponse of Graphene-Bi_2Te_3-FBG Heterostructure

Figure 4a shows the power (10^{-6}–10^{-3} W) dependent photoresponse of graphene-Bi_2Te_3-FBG heterostructure for broadband photodetection (400–1550 nm). Similar to graphene-FBG device, the increase in the incident power increases the photon–electron coupling in the graphene-Bi_2Te_3-FBG heterostructure and consequently results in increase in the Bragg wavelength shift.

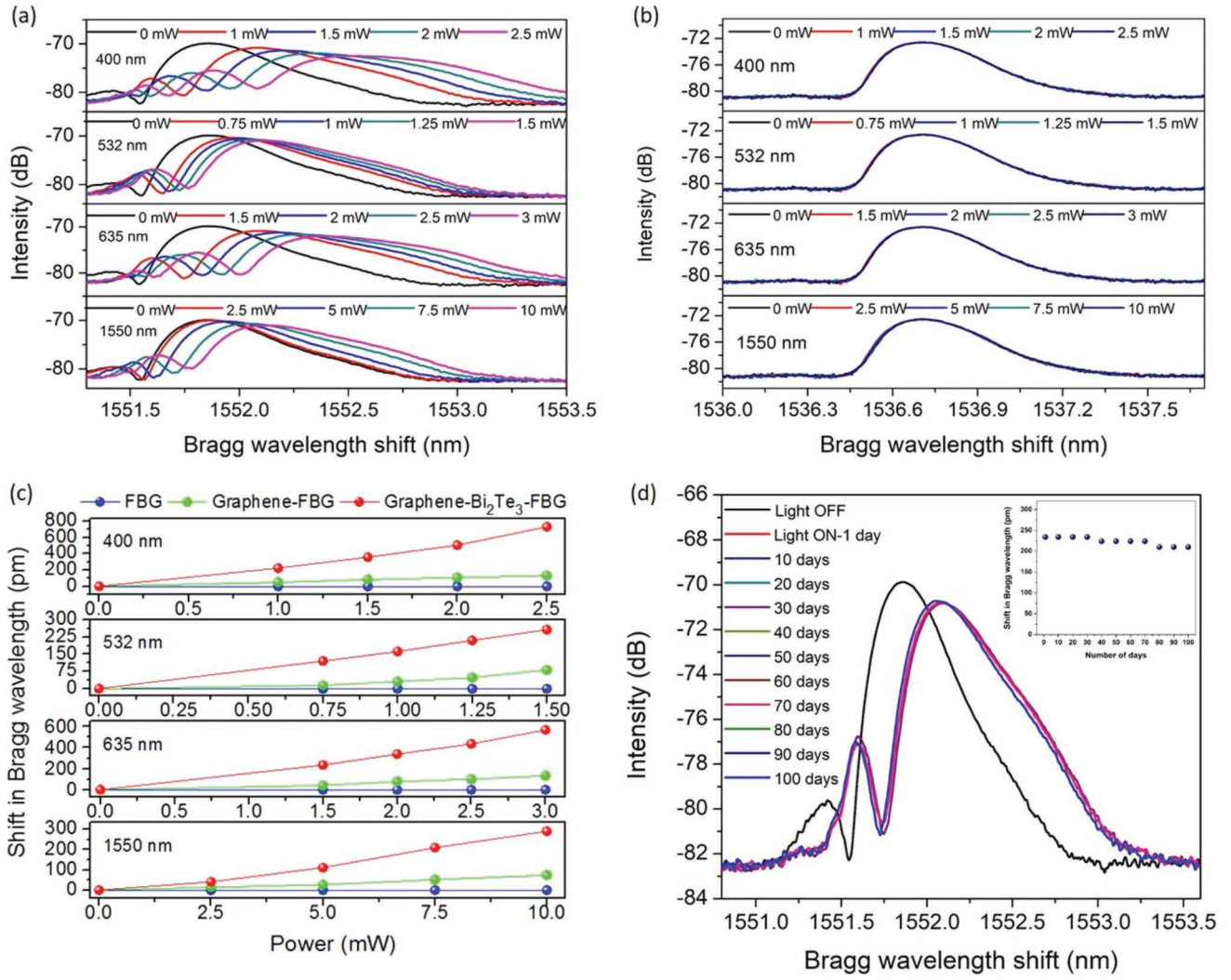

Figure 4. Power dependent photoresponse and long-term stability of graphene-Bi_2Te_3-FBG heterostructure photodetector. a) The redshift in the Bragg wavelength of graphene-Bi_2Te_3-FBG heterostructure photodetector increases with increase in the incident power of different wavelengths (400–1550 nm). b) There is no much shift in the Bragg wavelength of bare FBG with increase in the incident power of different wavelengths (400–1550 nm). c) The increase in shift in the Bragg wavelength of graphene-Bi_2Te_3-FBG heterostructure in comparison with graphene-FBG and bare FBG as a function of the increase in the incident optical power of different wavelengths. d) Long-term photoresponse stability of graphene-Bi_2Te_3-FBG device performance for about 100 d under ambient conditions.

We have repeated power (10^{-6}–10^{-3} W) dependent photoresponse on bare FBG for broadband wavelength (400–1550 nm) as shown in Figure 4b. Negligible Bragg wavelength shift was observed across a broadband wavelengths range (400–1550 nm) on the bare FBG, this result confirms that graphene and graphene-Bi_2Te_3 heterostructure are playing a key role in the photodetection. The power-dependent Bragg wavelength shift of graphene-Bi_2Te_3-FBG heterostructure is much greater than graphene-FBG at different wavelengths (400–1550 nm) as revealed in Figure 4c. Moreover, the Bragg wavelength shift can be tuned and modulated in picometer resolution (0–731 pm) by tuning the incident light power (10^{-6}–10^{-3} W). The maximum photosensitivity of graphene-Bi_2Te_3-FBG heterostructure device was found to be 740 pm mW^{-1} with the limit of detection (LoD) of 27 μW. We believe that the photosensitivity could be further increased by thinning or removing the cladding of the FBG device or by introducing plasmonic structures to enhance the absorption of graphene-Bi_2Te_3. This novel graphene and related 2D material integrated ultrabroadband photo-optic device (controlling light with light) has great potential to replace traditional silicon based electro-optic modulator[39] (controlling light with electric field) device.

We have also studied long-term photoresponse stability of graphene-Bi_2Te_3-FBG device performance for about 100 d as presented in Figure 4d. The graphene-Bi_2Te_3-FBG device shows slight shift in the Bragg wavelength from 234 to 210 pm even after 100 d under the illumination of laser light (635 nm, 1.5 mW). The slight shift in the Bragg wavelength was ≈10%, suggesting that graphene-Bi_2Te_3 integrated optical FBG device shows superior photoresponse stability.

3. Conclusion

In this work, we have demonstrated tracking and detecting the motion of light (millimeter precision) by integrating graphene with an optical FBG device. We have also demonstrated graphene integrated FBG device for ultrabroadband wavelength (400 nm to 10.768 µm) light detection with linear response. In addition, we have demonstrated that graphene-Bi_2Te_3-FBG heterostructure has much larger photoresponse which is 87% higher than graphene-FBG at both visible and telecom wavelengths. Finally, graphene-Bi_2Te_3-FBG heterostructure integrated optical FBG device shows superior stability even after 100 d under atmosphere condition. This concept may be further explored by coating other 2D materials (black phosphorous, transition metal dichalcogenides, topological insulators, boron nitride, and perovskites) on various optical fiber devices for light motion tracking in nanometer (nm) scale and ultrabroadband wavelength detection. This would be applicable to possible industrial applications such as machine vision, laser-based navigation and localization, humanoid robotics and robotic security devices by measuring laser light reflected from target objects.

4. Experimental Section

Synthesis of Graphene and Graphene-Bi_2Te_3 Heterostructure: High-quality, graphene monolayer was synthesized on copper (Cu) foil (Alfa Aesar, United States) using a typical chemical vapor deposition (CVD) method.[23,24] Bi_2Te_3 2D material was synthesized by physical vapor deposition method. During the process, high purity (99.99%) Bi_2Te_3 powder (Alfa Aesar, United States) was positioned in the center of the furnace with a temperature of 500 °C as the source material for evaporation, and graphene/Cu foil was positioned in the downstream with a temperature of 290–360 °C. Argon gas was used to carry the Bi_2Te_3 vapor onto the graphene film which resulted in graphene-Bi_2Te_3 heterostructure.

Characterizations of the Graphene and Graphene-Bi_2Te_3 Heterostructure: The graphene-FBG morphology was inspected by using optical microscopy (Nikon Eclipse, LV100ND). The graphene-Bi_2Te_3 heterostructure morphology was examined by using scanning electron microscope (FEI Quanta 200 FEG). Raman spectroscopy was measured with an excitation wavelength of 514 nm by using a micro-Raman system (Horiba Jobin Yvon, LabRAM HR 800). Atomic force microscope (Bruker, Dimension Icon) was used to examine the thicknesses of graphene and graphene-Bi_2Te_3 heterostructures. The broadband absorption spectrum of single-layer graphene and graphene-Bi_2Te_3 heterostructure were investigated by using a UV–vis-IR spectrometer (Newport, Pviv-211v, with a Keithley 2612).

FBG Device Fabrication and Experimental Setup: The FBG device was inscribed in a photosensitive germania doped silica fiber (core diameter: 8 µm and cladding diameter: 125 µm) using a phase mask method.[25,26] The experimental setup for light motion tracking and detecting consists of an external light sources with displacement stage, graphene-FBG device, circulator (1550 nm), broadband (400 to 2000 nm) supercontinuum laser source, and optical spectrum analyzer (Yokogawa AQ6370D) with high resolution of 20 pm.

Graphene-FBG Device Fabrication and Characterization: Graphene-FBG device was fabricated by transferring the CVD-grown graphene onto the optical FBG device, as shown in Figure S1 in the Supporting Information. First, poly(methyl methacrylate) (PMMA) polymer was deposited onto the upper surface of the graphene/Cu foil by spin coating method, devising PMMA/graphene/Cu heterostructure, where PMMA polymer film acted as a shielding layer to avoid breaking the graphene film until it is safely transferred onto the FBG device. The bottom layer of Cu foil was then thoroughly removed from the PMMA/graphene/Cu heterostructure by exposed to 1 M ferric chloride ($FeCl_3$) solution for 40 min. The PMMA/graphene film was washed three to four times with deionized water to remove any Cu foil residues, then transferred carefully onto the FBG device. The top layer of the PMMA polymer is removed from the graphene by treating with acetone for 12 h. After lifting, ultrafast laser was used to remove extra graphene from FBG device. Finally, single-layer graphene was coated on the top surface of optical FBG to fabricate a graphene-FBG device. The above method is followed even for fabricating graphene-Bi_2Te_3-FBG heterostructure device.

Optical Measurements: Light induced Bragg wavelength shift of graphene-FBG photodetector and graphene-Bi_2Te_3-FBG heterostructure photodetector measurements at visible and near-infrared wavelength range were accomplished on optical table using an optical spectrum analyzer (Yokogawa, AQ6370C). Light induced Bragg wavelength shift of graphene-FBG photodetector measurements at mid-infrared and far-infrared wavelength range were conducted on an optical microscopy platform (NeaSpec). The confocal micro-Raman system (WITec alpha 300R) was used to examine the Raman mapping measurements.

Supporting Information

Supporting Information is available from the Wiley Online Library or from the author.

Acknowledgements

The authors acknowledge financial support from Shenzhen Nanshan District Pilotage Team Program (LHTD20170006), the Science and Technology Innovation Commission of Shenzhen (Grant No. JCYJ20170818141429525), National Natural Science Foundation of China (Nos. 61604102, 51222208, 61875139, and 91433107), the National Key Research & Development Program (No. 2016YFA0201902 and 2016YFC0800500), the Interdisciplinary Research Support Scheme and Engineering Linkage Seed Fund Scheme at Monash University, and the Australian Research Council (IH150100006, FT150100450, and CE170100039).

Conflict of Interest

The authors declare no conflict of interest.

Keywords

2D materials, graphene, heterostructures, light motion tracking, optical fiber Bragg grating, ultrabroadband photodetection

Received: October 15, 2018
Revised: March 3, 2019
Published online:

[1] H. Mousazadeh, A. Keyhani, A. Javadi, H. Mobli, K. Abrinia, A. Sharifi, *Renewable Sustainable Energy Rev.* **2009**, *13*, 1800.
[2] M. Mahmoudpour, A. Zabihollah, M. Vesaghi, M. Kolbadinejad, *Microelectron. Eng.* **2014**, *119*, 37.
[3] G. Gariepy, N. Krstajić, R. Henderson, C. Li, R. R. Thomson, G. S. Buller, B. Heshmat, R. Raskar, J. Leach, D. Faccio, *Nat. Commun.* **2015**, *6*, 6021.
[4] A. K. Geim, K. S. Novoselov, *Nat. Mater.* **2007**, *6*, 183.

[5] K. S. Novoselov, A. K. Geim, S. V. Morozov, D. Jiang, Y. Zhang, S. V. Dubonos, I. V. Grigorieva, A. A. Firsov, *Science* **2004**, *306*, 666.
[6] R. R. Nair, P. Blake, A. N. Grigorenko, K. S. Novoselov, T. J. Booth, T. Stauber, N. M. R. Peres, A. K. Geim, *Science* **2008**, *320*, 1308.
[7] F. Bonaccorso, Z. Sun, T. Hasan, A. C. Ferrari, *Nat. Photonics* **2010**, *4*, 611.
[8] Q. Bao, K. P. Loh, *ACS Nano* **2012**, *6*, 3677.
[9] F. Xia, H. Wang, D. Xiao, M. Dubey, A. Ramasubramaniam, *Nat. Photonics* **2014**, *8*, 899.
[10] Q. Bao, H. Zhang, Y. Wang, Z. Ni, Y. Yan, Z. X. Shen, K. P. Loh, D. Y. Tang, *Adv. Funct. Mater.* **2009**, *19*, 3077.
[11] P. Li, Y. Chen, T. Yang, Z. Wang, H. Lin, Y. Xu, L. Li, H. Mu, B. N. Shivananju, Y. Zhang, Q. Zhang, A. Pan, S. Li, D. Tang, B. Jia, H. Zhang, Q. Bao, *ACS Appl. Mater. Interfaces* **2017**, *9*, 12759.
[12] F. H. L. Koppens, T. Mueller, Ph. Avouris, A. C. Ferrari, M. S. Vitiello, M. Polini, *Nat. Nanotechnol.* **2014**, *9*, 780.
[13] C. Xie, C. Mak, X. Tao, F. Yan, *Adv. Funct. Mater.* **2017**, *27*, 1603886.
[14] Y. H. Lu, S. R. Feng, Z. Q. Wu, Y. X. Gao, J. L. Yang, Y. J. Zhang, Z. Z. Hao, J. F. Li, E. P. Li, H. S. Chen, S. S. Lin, *Nano Energy* **2018**, *47*, 140.
[15] T. H. Han, Y. Lee, M. R Choi, S. H. Woo, S. H. Bae, B. H. Hong, J. H. Ahn, T. W. Lee, *Nat. Photonics* **2012**, *6*, 105.
[16] Z. Sun, A. Martinez, F. Wang, *Nat. Photonics* **2016**, *10*, 227.
[17] J. H. Chen, B. C. Zheng, G. H. Shao, S. J. Ge, F. Xu, Y. Q. Lu, *Light: Sci. Appl.* **2015**, *4*, e360.
[18] Q. Bao, H. Zhang, B. Wang, Z. Ni, C. H. Y. X. Lim, Y. Wang, D. Y. Tang, K. P. Loh, *Nat. Photonics* **2011**, *5*, 411.
[19] Q. Xu, T. Ma, M. Danesh, B. N. Shivananju, S. Gan, J. Song, C. W. Qiu, H. M. Cheng, W. Ren, Q. Bao, *Light: Sci. Appl.* **2017**, *6*, e16204.
[20] T. Low, A. Chaves, J. D. Caldwell, A. Kumar, N. X. Fang, P. Avouris, T. F. Heinz, F. Guinea, L. M. Moreno, F. Koppens, *Nat. Mater.* **2017**, *16*, 182.
[21] W. Li, B. Chen, C. Meng, W. Fang, Y. Xiao, X. Li, Z. Hu, Y. Xu, L. Tong, H. Wang, W. Liu, J. Bao, Y. R. Shen, *Nano Lett.* **2014**, *14*, 955.
[22] B. N. Shivananju, W. Yu, Y. Liu, Y. Zhang, B. Lin, S. Li, Q. Bao, *Adv. Funct. Mater.* **2017**, *27*, 1603918.
[23] Y. Zhang, L. Zhang, C. Zhou, *Acc. Chem. Res.* **2013**, *46*, 2329.
[24] X. Chena, L. Zhangb, S. Chena, *Synth. Met.* **2015**, *210*, 95.
[25] A. Othonos, *Rev. Sci. Instrum.* **1997**, *68*, 4309.
[26] B. N. Shivananju, A. Suri, S. Asokan, A. Misra. *Appl. Phys. Lett.* **2014**, *104*, 013104.
[27] B. C. Yao, Y. Wu, A. Q. Zhang, Y. J. Rao, Z. G. Wang, Y. Cheng, Y. Gong, W. L. Zhang, Y. F. Chen, K. S. Chiang, *Opt. Express* **2014**, *22*, 28154.
[28] J. Bonefacino, H. Y. Tam, T. S. Glen, X. Cheng, C. F. P. Pun, *Light: Sci. Appl.* **2018**, *7*, 17161.
[29] A. D. Sanctis, G. F. Jones, D. J. Wehenkel, F. Bezares, F. H. L. Koppens, M. F. Craciun, S. Russo, *Sci. Adv.* **2017**, *3*, e1602617.
[30] S. Goossens, G. Navickaite, C. Monasterio, S. Gupta, J. J. Piqueras, R. Pérez, G. Burwell, I. Nikitskiy, T. Lasanta, T. Galán, E. Puma, A. Centeno, A. Pesquera, A. Zurutuza, G. Konstantatos, F. Koppens, *Nat. Photonics* **2017**, *11*, 366.
[31] B. N. Shivananju, A. Suri, S. Asokan, A. Misra, *Rev. Sci. Instrum.* **2013**, *84*, 095101.
[32] B. N. Shivananju, S. Asokan, A. Misra, *J. Phys. D: Appl. Phys.* **2015**, *48*, 275502.
[33] Y. Zhang, T. Liu, B. Meng, X. Li, G. Liang, X. Hu, Q. J. Wang, *Nat. Commun.* **2013**, *4*, 1811.
[34] C. H. Liu, Y. C. Chang, T. B. Norris, Z. Zhong, *Nat. Nanotechnol.* **2014**, *9*, 273.
[35] B. N. Shivananju, M. Renilkumar, G. R. Prashanth, S. Asokan, M. M. Varma, *J. Lightwave Technol.* **2013**, *31*, 2441.
[36] B. N. Shivananju, S. Yamdagni, R. Fazuldeen, A. K. S. Kumar, G. M. Hegde, M. M. Varma, S. Asokan, *Rev. Sci. Instrum.* **2013**, *84*, 065002.
[37] H. Qiao, J. Yuan, Z. Xu, C. Chen, S. Lin, Y. Wang, J. Song, Y. Liu, Q. Khan, H. Y. Hoh, C. X. Pan, S. Li, Q. Bao, *ACS Nano* **2015**, *9*, 1886.
[38] H. Mu, Z. Wang, J. Yuan, S. Xiao, C. Chen, Y. Chen, Y. Chen, J. Song, Y. Wang, Y. Xue, H. Zhang, Q. Bao, *ACS Photonics* **2015**, *2*, 832.
[39] G. T. Reed, G. Mashanovich, F. Y. Gardes, D. J. Thomson, *Nat. Photonics* **2010**, *4*, 526.